Earth and Planetary Science Letters 493 (2018) 128–139

Contents lists available at ScienceDirect

Earth and Planetary Science Letters

www.elsevier.com/locate/epsl

Vanadium isotope compositions of mid-ocean ridge lavas and altered oceanic crust

Fei Wu [a,b], Yuhan Qi [a], M.R. Perfit [c], Yongjun Gao [d], Charles H. Langmuir [e], V. Dorsey Wanless [f], Huimin Yu [a], Fang Huang [a,*]

[a] CAS Key Laboratory of Crust–Mantle Materials and Environments, School of Earth and Space Sciences, University of Science and Technology of China, Hefei, Anhui, China
[b] Department of Earth, Ocean and Atmospheric Science, Florida State University, Tallahassee, FL, USA
[c] Department of Geological Sciences, University of Florida, Gainesville, FL, USA
[d] Department of Earth and Atmospheric Sciences, University of Houston, Houston, TX, USA
[e] Department of Earth and Planetary Sciences, Harvard University, Cambridge, MA, USA
[f] Department of Geosciences, Boise State University, Boise, ID, USA

ARTICLE INFO

Article history:
Received 17 November 2017
Received in revised form 7 April 2018
Accepted 9 April 2018
Available online 26 April 2018
Editor: F. Moynier

Keywords:
vanadium isotopes
oceanic basalts
hydrothermal alteration
magmatic differentiation
oxygen fugacity

ABSTRACT

Vanadium isotope compositions of igneous rocks have the potential to constrain variations of physico-chemical conditions such as oxidation states during magmatism. Here, we present V isotope data for 27 fresh lavas (ranging from basaltic to dacitic compositions) from mid-ocean ridges, 31 altered basalts and gabbros from IODP site 1256 near the East Pacific Rise (EPR), and 2 back arc basin basalts (BABB). Our analyses of fresh mid-ocean ridge basalt (MORB) provide new constraints on the V isotope composition of MORBs, i.e. $\delta^{51}V = -0.84 \pm 0.02‰$ (2SE, $n = 22$). In addition, the mean $\delta^{51}V$ of MORBs from individual segments is correlated with the mean ridge depth and $Na_{8.0}$ of the segment, which might reflect the effect of melting extent on V isotope fractionation during mantle melting.

The mafic profile of intact altered oceanic crust (AOC) from the IODP site 1256 has $\delta^{51}V$ ranging from -1.01 to $-0.77‰$, similar to that of fresh MORBs, suggesting that V isotope fractionation is limited during alteration of oceanic crust. These results also indicate the V isotopic homogeneity of the bulk oceanic crust with average $\delta^{51}V$ of $-0.85 \pm 0.02‰$ (2SE, $n = 53$), which is unaffected by ocean water and hydrothermal fluid alteration. Our results provide a guideline for application of V isotopes into studies of low and high temperature geochemical processes.

The evolved lavas (basaltic andesites, andesites, and dacites) from the East Pacific Rise (EPR) show apparent shifts towards heavy $\delta^{51}V$ values with increasing degree of differentiation, which can be explained by the crystal–liquid fractionation during crystallization with an inferred isotope fractionation factor of $\Delta^{51}V_{mineral\text{-}melt} = -0.15 \times 10^6/T^2$. The enrichment of ^{51}V with increasing differentiation degree for the 9°N Overlapping Spreading Center (OSC) lavas is consistent with direction of the isotope shift observed in lavas from Anatahan Island (Northern Mariana Arc) and Hekla Volcano (Iceland), but the magnitude (0.3‰) is much smaller than that (2‰) reported in Prytulak et al. (2017). Modeling of V isotope fractionation between mineral and melt shows that variations in redox condition are important for controlling V isotope fractionation, but insufficient to explain the dramatically different $\Delta^{51}V_{mineral\text{-}melt}$ between 9°N OSC lavas and Anatahan/Hekla suites. More studies are necessary for better understanding of mechanisms of V isotope fractionation during magmatism.

1. Introduction

Vanadium (V) is a refractory, lithophile, and slightly siderophile transition metal element with multiple valence states (V^{5+}, V^{4+}, V^{3+}, V^{2+}, and V^0) (Huang et al., 2015). The speciation and partitioning of V in the planets, meteorites, and Moon are regulated by oxygen fugacity (fO_2). For this reason, V has been widely used to constrain variations of redox conditions during igneous processes. For example, the speciation of V in the glasses and minerals from planetary basalts and meteorites was applied to constrain the redox variations in the inner solar system (Karner et al., 2006; Righter et al., 2016). Vanadium concentrations of the bulk Earth

* Corresponding author.
E-mail address: fhuang@ustc.cn (F. Huang).

https://doi.org/10.1016/j.epsl.2018.04.009
0012-821X/

versus bulk silicate Earth (BSE) were applied to understand the conditions of terrestrial accretion and core formation (e.g. Siebert et al., 2013). The ratios of V to single valent elements with similar compatibility during mantle melting (such as Sc) have been used as a proxy for redox state variations of the mantle and crust (e.g. Lee et al., 2005; Mallmann and O'Neill, 2009; Laubier et al., 2014).

Vanadium has two stable isotopes, ^{51}V (99.76%) and ^{50}V (0.24%), which can be fractionated between coexisting species with different bond strengths and energies during redox-related processes (e.g. Schauble et al., 2004). This principle can also be applied to the V isotope system as shown recently by the theoretical study of Wu et al. (2015), providing the potential to fingerprint redox-state variations in nature. Owing to the advance of isotope analytical methods using multi-collector inductively coupled plasma mass spectrometry (MC-ICPMS), stable V isotopes can be measured with the precision necessary to identify natural V isotope variations (Nielsen et al., 2011, 2016; Prytulak et al., 2011; Wu et al., 2016). Recent studies have revealed significant V isotope fractionation during both low and high temperature processes (Gao et al., 2018; Prytulak et al., 2013, 2017; Schuth et al., 2017; Ventura et al., 2015; Wu et al., 2016), implying the promising application of V isotopes as a new tracer, especially of oxidation states in the rocky planets and Earth.

Prytulak et al. (2013) observed significant V isotope variations of peridotites with δ^{51}V ranging from −0.58‰ to −1.17‰, and suggested on this basis a bulk silicate Earth ("BSE value") of (-0.7 ± 0.2‰). Prytulak et al. (2017) further observed significant V isotope fractionation up to ∼2‰ during magmatic differentiation in Anatahan and Hekla lavas (Prytulak et al., 2017). In contrast, measurement of igneous silicate rock standards with a large range of SiO_2 (47–67 wt.%) including basalts and differentiated granitoids only showed small V isotope variations (∼0.33‰) (Wu et al., 2016). Thus, it is still not clear the magnitude and mechanism of V isotopes fractionation during magmatism, hindering the application of V isotope systematics to the studies of planetary mantle–crust differentiation. More investigations for igneous rocks with high-quality V isotope data are necessary to better understand V isotope fractionation during partial melting and magma differentiation.

The mid-ocean ridge (MOR) constitutes ∼75% of the total global erupted magma and created most of the oceanic crust (White and Klein, 2014). Mid-ocean ridge basalt (MORB) represents the most extensive crustal reservoir of the terrestrial Earth and they also provide critical genetic and compositional links to the upper mantle (Gale et al., 2013). Although Prytulak et al. (2013) presented V isotope data for several fresh and MORB samples, more data are needed to better constrain the V isotope composition of MORBs and oceanic crust. Here, we report high-precision V isotopic compositions for 27 well-characterized fresh MOR lavas with compositions from basaltic to dacitic, 2 back arc basin basalts (BABBs), and 31 mafic rocks of the altered oceanic crust (AOC) recovered from the IODP site 1256, which represent an intact section of oceanic crust near the East Pacific Rise (EPR). The purposes of this study are to (1) evaluate V isotope fractionation during magma differentiation at MORs, (2) examine the effect of fluid–rock interaction on the δ^{51}V of the AOC, and (3) estimate the average V isotope composition of MORB and oceanic crust. With these results, we can establish a benchmark for using V isotopes to trace differentiation process on the terrestrial Earth and rocky planets.

2. Sample description and geological background

2.1. Fresh MORB and BABB

Twenty MORB samples were measured in this study. They are predominantly N-MORBs from axial ridge sections including the EPR at 09–10°N, the Gakkel Ridge at 82–87°N, and the South East Indian Ridge at 50°S, with one E-MORB sample from Mid-Atlantic Ridge at 35°N. The full spreading rates of these ridge segments vary from less than 1.5 cm/yr for the Gakkel Ridge to about 11 cm/yr for the EPR (White and Klein, 2014). In addition, two BABB from the Lau Basin, a back-arc basin at the Australian–Pacific plate boundary, were also analyzed. All MORB and BABB samples are fresh lavas (Gale et al., 2013; Perfit et al., 2012; Wanless et al., 2010, 2012). More sample details (locations, elemental and radiogenic isotope compositions) are in the Supplementary materials. These samples span a broad range in elemental and radiogenic isotope compositions. Their MgO contents range from 5.93 to 9.08 wt.% and V from 214 to 406 ppm (Table S1). The trace element contents of these MORB range from typical N-MORB to E-MORB. The MOR basaltic andesites to dacites have MgO content from 5.98 to 0.08 wt% and V contents from 305 to 45 ppm.

2.2. AOC samples from IODP 1256

IODP site 1256 (6°44.2′N, 91°56.1′W) is located in the Guatemala Basin on the Cocos Plate, which was drilled into the oceanic crust that formed ∼15 m.y. ago on the eastern flank of the EPR during an episode of superfast spreading with rates up to 20 cm/yr (Wilson et al., 2006). Basement rocks were recovered from Hole 1256C and Hole 1256D after penetrating ∼250 m of sediments (Teagle et al., 2006). Hole 1256C is comprised of a 32 m thick lava pond between two thin sheet flows that underlie the 88.5 m thick sediment layer (Fig. 4). The main Hole 1256D started coring at 276 m below seafloor (mbsf) and penetrated 1271 m into the oceanic basement (Fig. 4).

The oceanic crust at the Hole 1256D is subdivided into four main lithological units from top to bottom based on the shipboard core observations (Teagle et al., 2006) and alteration processes (Alt et al., 2010), including a volcanic section (250–1004.2 mbsf), a transition zone (1004.2–1060.9 mbsf), a sheeted dike complex (1060.9–1406.6 mbsf), and a plutonic complex (1406.6–1521.3 mbsf) (Fig. 4). Lithostratigraphy and distribution of secondary minerals versus depth in Hole 1256D indicate an increase in the degree of hydrothermal alteration with depth, in accord with an increase in alteration temperatures (Fig. 4) (Alt et al., 2010). Low temperature alteration occurs mostly in the volcanic section with a range from ∼50 to 135 °C (Alt et al., 2010). The transition zone is characterized by greenschist and sub-greenschist minerals in rocks with alteration temperatures of ∼130–180 °C (Fig. 4) (Teagle et al., 2006; Alt et al., 2010). High temperature hydrothermal alteration occurred in the sheeted dyke complex due to circulation of high-temperature (∼400–850 °C) fluids (Alt et al., 2010). The underlying lowermost dyke complexes and plutonic complex underwent high temperature contact metamorphism caused by intrusion of gabbro bodies at ∼850–950 °C and is characterized by granoblastic textures (Koepke et al., 2008; Alt et al., 2010). In addition, the downhole pattern of bulk sample δ^{18}O and δ^{7}Li also reflect variations in water–rock ratio together with a downward increase of alteration temperature (Gao et al., 2012). Consequently, the Hole 1256D profile documents the transition from low temperature seawater alteration to high temperature hydrothermal alteration and contact metamorphism in the oceanic crust.

Thirty-one well-characterized samples from Site 1256 (one from hole 1256C and thirty from 1256D) were analyzed for V isotopic

compositions. These samples represent all rock types present in the core, covering six sections of the drilled oceanic crust, and spanning a broad range in depths from 258.5 to 1502.7 mbsf (Fig. 4). The studied samples have SiO_2 contents from 47.4 to 55.5 wt.%, MgO from 5.16 to 10.65 wt.%, V from 198 to 817 ppm, and $\delta^{18}O$ from 3.0‰ to 8.6‰ (Table S2) (Gao et al., 2012).

2.3. Evolved lavas from the MOR

The MOR evolved lavas are from the 9°N overlapping spreading center (OSC) which is located between the Clipperton and Siquieros transform faults on the EPR. It consists of two discontinuous north-south trending limbs separated by ~8 km with an overlap of ~27 km (Sempere and Macdonald, 1986). The eastern limb is propagating to the south into older crust at a rate of ~4.2 cm/yr (Carbotte and Macdonald, 1992). Geophysical studies showed that there are shallow melt lenses beneath both limbs of the OSC and in the inter-limb region north of the overlap basin, which indicates a high magma supply rate at this area (Kent et al., 2000). The 9°N OSC region has produced tholeiitic lavas ranging from basalt to dacite with a wide range of SiO_2 contents (~50–67 wt.%) (Wanless et al., 2010). Lavas with more evolved compositions (>56 wt.% silica) are confined to the eastern propagating limb of the OSC, where magmas are in contact with older volcanic crust (Wanless et al., 2010, 2011). Geochemical observations reveal that extensive fractional crystallization of N-MORB coupled with minor amounts of assimilation of partially altered crust are required to produce the range of compositions observed along the east limb of the OSC (Wanless et al., 2010, 2011).

3. Analytical methods

The details of the analytical methods for V isotopes are available in Wu et al. (2016). A brief description of the chemical separation and measurement protocol is provided here. Sample powders containing approximately 5–10 μg of V were digested with a 3:1 (v/v) mixture of concentrated HF–HNO_3 mixture. After the full digestion, the samples were treated by aqua regia and concentrated HNO_3 to remove F^-, then dissolved in 1 mL 1 mol L^{-1} HNO_3 for ion-exchange chromatography.

Chemical purification of V was conducted with a multi-step ion-exchange procedure using cation- and anion-exchange columns. The cation resin AG50W-X12 (200–400 mesh) was applied to remove Fe, Ti, and other major matrix elements (e.g. Al, Ca, Mn, and Cr). Then AG1-X8 (200–400 mesh) anion resin was further used to remove residual matrix and isobaric elements (e.g. K, Na, Mg, and trace amount of Cr). The total procedure blank was less than 2 ng; negligible compared with the loaded amount of V (5–10 μg). The V yields of the total chemical procedures were >99%. V isotopic ratios were measured using a sample-standard bracketing method on a Neptune Plus (Thermo-Fisher Scientific) MC-ICP-MS at USTC using an Aridus II desolvator (CETAC Technologies) system. The typical sensitivity of ^{51}V was ~150 V/ppm with a 10^{10} Ω amplifier under a medium resolution mode. We measured ^{49}Ti and ^{53}Cr to precisely correct for the interferences of ^{50}Ti and ^{50}Cr on ^{50}V. Vanadium isotopic data are reported in a δ notation in per mil against the international reference material AA (Nielsen et al., 2011):

$$\delta^{51}V = \left(\left({}^{51}V/{}^{50}V\right)_{sample}/\left({}^{51}V/{}^{50}V\right)_{AA} - 1\right) \times 1000(‰) \quad (1)$$

The data quality of V isotope analyses was rigorously monitored using a number of in-house standards, international reference materials, and duplicated samples. The $\delta^{51}V$ of the rock standards are in good agreement with the literature values (Table S1). The reproducibility of $\delta^{51}V$ for rock standards and duplicate samples are better than 0.10‰ (2SD). Five samples were replicated by digestion of separate rock powders, all showing good reproducibility in $\delta^{51}V$ (Table S1 and Table S2). These results prove the reliability of our V isotope data.

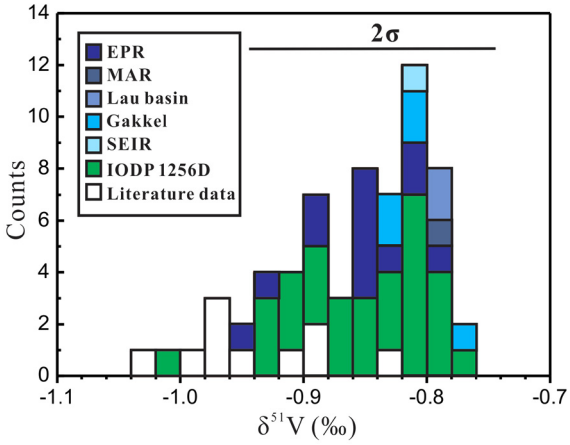

Fig. 1. The histogram of V isotopic compositions of MORB, BABB, and altered oceanic crust (AOC) from IODP Site 1256 measured in this study. Data are reported in Tables S1 and S2. Literature data of MORB are from Prytulak et al. (2013). (For interpretation of the colors in the figure(s), the reader is referred to the web version of this article.)

4. Results

Vanadium isotopic compositions of the fresh MORB and BABB glass samples are reported in Table S1 and shown in Fig. 1. The $\delta^{51}V$ values of these samples range from −0.96 to −0.76‰. There are systematic variations among different regions. The $\delta^{51}V$ varies from −0.96 to −0.80‰ in EPR N-MORB ($n = 13$), from −0.83 to −0.76‰ in Gakkel Ridge N-MORBs ($n = 5$), and from −0.80 to −0.79‰ in the Lau Basin ($n = 2$). The N-MORB from the South East Indian Ridge has $\delta^{51}V$ value of -0.80 ± 0.05‰, and the E-MORB from the mid-Atlantic Ridge has a value of -0.79 ± 0.04‰. These values are systematically heavier, although within error of fresh MORB glass samples published previously (−1.04 to −0.84‰, $n = 6$; Prytulak et al., 2013, see Fig. 1).

All samples from IODP Site 1256 are reported in Table S1 and Fig. 1. The $\delta^{51}V$ values of these rocks range from −1.01 to −0.77‰, with an average value of -0.85 ± 0.02‰ (2SE, $n = 31$). These values agree well with the data for fresh EPR MORBs reported here.

Vanadium isotopic compositions of the andesitic to dacitic lavas from 9°N OSC on the EPR are in Table S1. Except for one basaltic andesite with higher MgO content (5.98 wt.%) and lighter V isotopic composition ($\delta^{51}V = -0.87 \pm 0.04$‰), the $\delta^{51}V$ values of the other samples range from −0.74 to −0.64‰, with an average value of -0.71 ± 0.03‰ (2SE, $n = 6$). These values are considerably lower than that of more primitive MORB.

5. Discussion

5.1. V isotope composition of MORBs

The basaltic ocean ridge samples reported here include N-MORB, E-MORB, and BABB spanning a large range in geographical distribution and chemical composition. If one considers all ridge basalt samples as a single group, then there is a systematic difference between the new data reported here and those from Prytulak et al. (2013). The mean $\delta^{51}V$ of our samples with the exception of the differentiated samples discussed below is -0.84 ± 0.02‰ (2SE, $n = 22$), while the mean of Prytulak et al. (2013) is -0.95 ± 0.04‰ (2SE, $n = 10$) (Fig. 1 and Fig. 2). Fig. 2 also demonstrates that

Table 1
Depth and average $Na_{8.0}$ for sampling segments and the average $\delta^{51}V$ values of samples from each segment.

Ridge	Mean $Na_{8.0}$ (%)	SE	Mean $\delta^{51}V$ (‰)	2SE	N[a]	Depth (m)	Reference[b]
Kolbeinsey Ridge	1.9	0.06	−0.95	0.07	5	−300	Klein and Langmuir (1987)
ODP 801C (Pacific Ocean)	2.21	0.16	−0.93	0.05	4		Fisk and Kelley (2002)
East Pacific Rise	2.68	0.03	−0.86	0.03	13	−2589	Wanless et al. (2012)
Central Indian Ridge	2.71		−0.99	0.17	1	−2710	Gannoun et al. (2007)
South East Indian Ridge	2.91		−0.8	0.10	1	−3400	Gale et al. (2014)
Gakkel Ridge 1	3.02	0.03	−0.81	0.01	3	−3900	Gale et al. (2014)
Gakkel Ridge 2	3.35		−0.79	0.06	2	−4600	Gale et al. (2014)

[a] N represents the numbers of sample from each segment. For segment with $N > 1$, the mean $\delta^{51}V$ and 2SE were calculated with the average value and standard error of mean of the results of N samples. For segment with $N = 1$, we use the long-term external precision of the measurement (0.10‰ for our data and 0.17‰ for data from Prytulak et al., 2013) to represent the error.

[b] References for the segment information (depth and mean $Na_{8.0}$) of the samples.

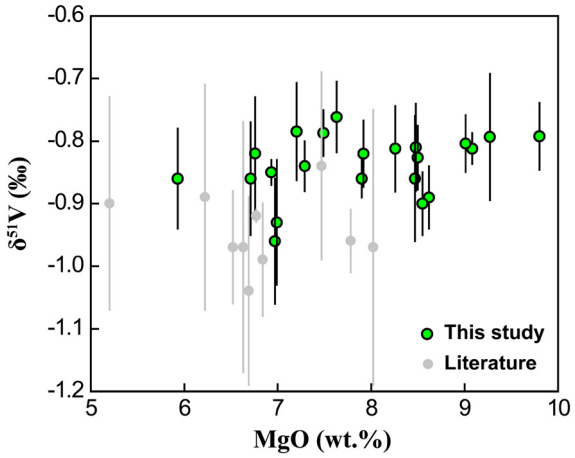

Fig. 2. MgO versus $\delta^{51}V$ in the studied MORBs and BABBs from this study and literature (Prytulak et al., 2013). Note that there is no correlation between MgO and $\delta^{51}V$ in each data set, yet these is an isotopic offset between the two data sets.

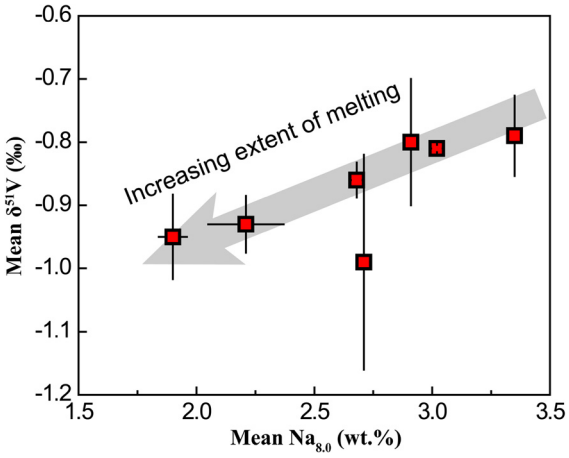

Fig. 3. Average $Na_{8.0}$ versus $\delta^{51}V$ in N-MORBs using segment means from different ridge segments. Averages can be found in Table 1. Error bars are two standard error of the mean for segments with more than one sample and the long term analytic uncertainty (0.10‰ for our data and 0.17‰ for data from Prytulak et al., 2013) when there is only one measurement.

in both data sets with limited fractional crystallization of MORBs (Mg# >50), $\delta^{51}V$ do not vary with MgO content. Thus, the V isotope differences between the present and previous work cannot result from magma differentiation. One possibility could be inter-laboratory bias, but because the V isotope analyses of most basaltic standard materials (except BCR-2, see Wu et al., 2016) from the present and earlier studies give results consistent within error, it is too early to make such conclusions.

The alternative explanation is that these differences reflect real variations among MORBs. Prytulak et al. (2013) analyzed zero age samples largely from the Kolbeinsey rise adjacent to Iceland with a ridge depth of only 500 m and a $Na_{8.0}$ values of less than 2.00% (Klein and Langmuir, 1987). These samples are not representative of MORB as a whole, since this segment from Kolbeinsey rise is an extreme case in global MOR systems (see Gale et al., 2013). The other samples from ancient crust at ODP site 801C also have lower $Na_{8.0}$ compared to the average ocean ridges (Fisk and Kelley, 2002). In contrast, samples analyzed in this study span ridge depths from 2500 to 4500 m and $Na_{8.0}$ from 2.65 to 3.50%.

Because the range of V isotope compositions is small, we can follow the approach of Gale et al. (2013) and use segment means of the data to obtain higher precision for regional differences. We exclude the extreme E-MORB sample from the Atlantic and the back-arc basin samples for the regional comparison since they have different mantle source. The results are as shown in Table 1. Segment mean $Na_{8.0}$ from Gale et al. (2013) is plotted against the average $\delta^{51}V$ in Fig. 3. For segments with only one sample, the error is as large as the analytic uncertainty on single measurements, while mean values with multiple samples have a much smaller standard error of mean. A line drawn through the more precise values includes the error bars for segments with single measurements, implying that V isotope compositions of MORB vary along ocean ridges and they are correlated with $Na_{8.0}$ and axial depth (Fig. 3).

Previous studies demonstrated that variations in MORB chemical composition, ridge depth, and the underlying seismic velocities in the underlying mantle are all consistent with potential temperature differences of about 200 °C, which would lead to large variations in the extent of melting of the mantle beneath ridges (e.g. Dalton et al., 2014; Gale et al., 2014; Klein and Langmuir, 1987). In this case, V isotope composition of MORB could initially be heavier than the mantle source, and become increasingly light as the melting extent increases. One would then expect that abyssal peridotites become increasingly light in V isotope composition as higher extents of melt are extracted.

These observations potentially reconcile the differences between the present measurements and the results from Prytulak et al. (2013). The differences might reflect real variations in $\delta^{51}V$ that respond to the melting extent of the underlying mantle. The "mean MORB" value should then reflect MORB from the mean depth of the ridge. Because the EPR has the mean depth of the ridge similar to that of the "mean MORB" (Gale et al., 2013), the V isotope composition of EPR MORBs reported here should be representative of average MORB compositions, which have $\delta^{51}V$ of -0.86 ± 0.03‰ (2SE, $n = 13$), significantly different from the estimation from Prytulak et al. (2013).

It is also possible that the systematic difference reflects the relative high uncertainty (0.17‰, 2SD) of V isotope measurement by previous work (Prytulak et al., 2013). If so, because the E-MORB and BABB have $\delta^{51}V$ values comparable to N-MORB, one could ar-

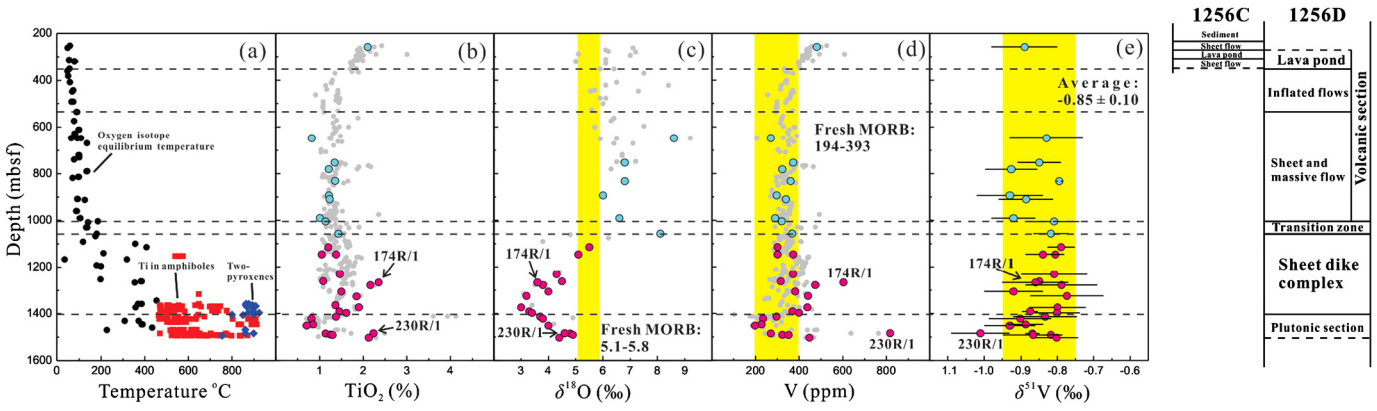

Fig. 4. Downhole variations of (a) alteration temperatures, (b) TiO_2 contents, (c) $\delta^{18}O$, (d) V contents, and (e) $\delta^{51}V$ through the oceanic crust at IODP Site 1256. Alteration temperatures were estimated from mineral-water oxygen isotope thermometer, fluid inclusions, Ti-in-amphibole and two-pyroxenes geothermometry (Alt et al., 2010). The colored bar in (c) shows the range of $\delta^{18}O$ in fresh MORB (Eiler et al., 2000). The colored bar in (c) denote the range of V in fresh MORB (Gale et al., 2013). TiO_2 and V contents are from Gao et al. (2009), and $\delta^{18}O$ are from Gao et al. (2012).

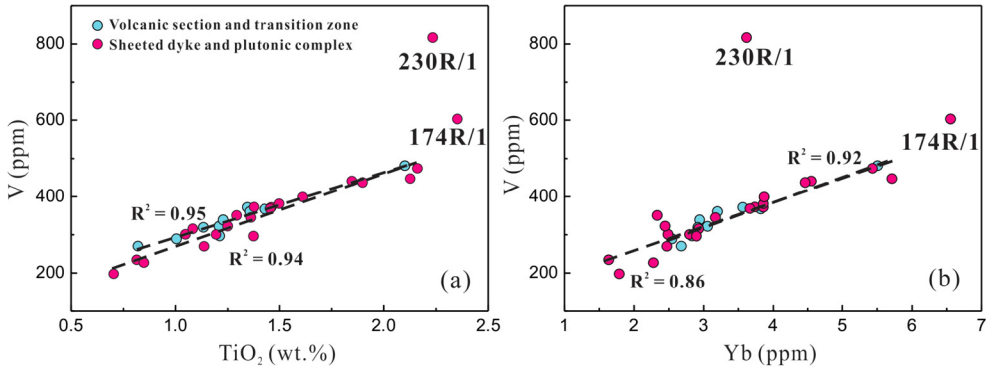

Fig. 5. (a) TiO_2 versus V, and (b) Yb versus V in the studied AOC samples at IODP Site 1256. The TiO_2, Yb and V contents are from Gao et al. (2009). The dashed line represents the best-fit linear regression for low temperature AOC samples from volcanic section and transition zone at IODP Site 1256, and high temperature AOC samples from sheeted dyke and plutonic complex IODP Site 1256 (except samples 230R/1 and 174R/1).

gue for overall homogeneity in $\delta^{51}V$. Then the mean value of $\delta^{51}V$ based on our new data would be -0.84 ± 0.02‰ (2SE, $n = 22$), indistinguishable from the EPR value given above. In any case, our high-quality data for more representative samples provide the currently best constraint on the V isotope composition of the MORB.

The observed relationship between mean $Na_{8.0}$ and average $\delta^{51}V$ of the N-MORBs (Fig. 3), if it is substantiated, further indicates that V isotopes are fractionated during mantle melting, and the extracted melt is enriched in the heavy isotope. This is consistent with the plausible melt extraction trend observed by Prytulak et al. (2013). However, all the observed $\delta^{51}V$ values of MORB (-1.06 to -0.76‰) are lighter than the reference V isotope composition of the BSE as proposed by Prytulak et al. (2013) (-0.7 ± 0.2‰). In addition, the observed $\delta^{51}V$ values of MORB are also generally lighter than the abyssal peridotites without intense post alteration (-0.66 to -0.84‰ from Prytulak et al., 2013), although the analytical precision (0.17‰, 2SD) for V isotope data of peridotites does not allow to fully resolve such small fractionation. These results imply that either some process modified V isotope composition of mantle source of the MORB and other processes modified V isotope composition of abyssal peridotites after initial melting extraction. Or more possibly, the high-quality V isotope date of more peridotite samples are needed to better constrain the V isotope composition of the BSE.

5.2. V isotope behavior during hydrothermal alteration in AOC

The samples collected from Hole 1256D include an intact sequence of oceanic crust through lavas, dikes, and uppermost gabbros. These basalts and gabbros vary from primitive to relatively differentiated compositions with SiO_2 from 47.4 to 53.2 wt.% and Mg# from 69.4 to 37.5 (Wilson et al., 2006). In addition, detailed mineralogy and geochemical investigations reveal that the Hole 1256D profile records the transition from low temperature alteration to high temperature hydrothermal alteration (Alt and Teagle, 2000; Gao et al., 2012; Teagle et al., 2006). The bulk $\delta^{18}O$ values of igneous rocks in hole 1256D range from 3.0 to 9.2‰, which reflects the influence of hydrothermal alteration and seafloor weathering processes at different temperatures and depths (Alt and Teagle, 2000; Gao et al., 2012). The basalts from the uppermost volcanic section and transition zone (<1060.9 mbsf) have higher $\delta^{18}O$ (6.0‰ to 9.2‰) than fresh MORB (5.3‰ to 5.8‰, Eiler et al., 2000), reflecting the interaction between seawater and oceanic crust at temperatures lower than 250°C, while the low $\delta^{18}O$ of igneous rocks (3.0‰ to 5.5‰) recovered below the transition zone (>1060.9 mbsf) are due to high temperature (>250 °C) hydrothermal alteration (Fig. 4) (e.g. Alt and Teagle, 2000; Teagle et al., 2006).

The volcanic section and transition zone (<1060.9 mbsf) exhibit slight to moderate seawater alteration below 250 °C (Alt et al., 2010; Gao et al., 2012). Most of the altered basalts above the transition zone have restricted variations of V abundances (270–370 ppm, Fig. 4) around the mean value of the fresh MORB (309 ppm) (Gale et al., 2013; Huang et al., 2015). In addition, V contents in these samples are correlated with elements insensitive to oceanic alteration such as Ti and rare earth elements (Fig. 5), implying that seawater alteration is not the reason for the small V content variations in these zones. Instead, such correla-

tions more likely reflect different extents of fractional crystallization of parental magmas (Wilson et al., 2006). Thus, V is relatively immobile in the seawater alteration zones of IODP 1256 section at temperature <250 °C, which is consistent with the previous experimental study showing that V has low solubility in fluids at temperatures <300 °C during seawater alteration of basalt (Seyfried and Mottl, 1982). The conservative behavior of V at low temperatures may be responsible for the limited range of δ^{51}V in the volcanic section and transition zone rocks (−0.81‰ to −0.93‰, Fig. 4), which is indistinguishable to fresh EPR MORB (−0.78‰ to −0.96‰, Fig. 1). Such results are consistent with previous study on the discrete AOC samples from ODP Sites 801 and 1149 (Prytulak et al., 2013). Consequently, low temperature alteration does not appear to modify V isotope signatures in the mafic oceanic crust.

In the sheeted dikes and plutonic complex below the transition zone, high temperature alteration with hydrothermal fluids occurred to various extents, along with contact metamorphic recrystallization and hydrous partial melting (Alt et al., 2010; Koepke et al., 2008). Vanadium concentrations are more variable in the sheeted dykes and the plutonic complex than the overlying volcanic section and transition zone (198–817 ppm, Fig. 4). The V contents for most samples are likely controlled by crystallization, but 174R/1 (1266.7 mbsf) and 230R/1 (1483.68 mbsf) show abnormally high V contents (603 and 817 ppm) outlying the general trend between V and elements insensitive to oceanic alteration (Fig. 5). Detailed petrographic observation showed that the gabbro samples from plutonic section commonly carry Fe–Ti oxide (Yamazaki et al., 2009). However, there is lack of evidence from either petrography (Yamazaki et al., 2009) or geochemistry (Fe–Ti–V–Mg contents, Neo et al., 2009; Gao et al., 2009) that sample 174R/1 and 230R/1 has extra cumulate Fe–Ti oxides. Thus, the abnormal enrichment of V in these samples is hard to result from Fe–Ti oxide accumulation, although such possibility exists. On the other hand, the V content in these samples may be due to enrichment by hydrothermal alteration. Despite the variable extent of hydrothermal alteration, the altered mafic rocks in the sheeted dikes and plutonic complex have restricted δ^{51}V, indistinguishable from overlying low-temperature altered basalts and fresh MORBs from the EPR (Fig. 1 and Fig. 4). In addition, sample 230R/1 with high V content (817 ppm) has δ^{51}V value (−1.01‰) only slightly lighter than the other samples in IODP 1256, although the cause of V enrichment in these samples is unclear. Thus high-temperature hydrothermal alteration in the AOC at IODP 1256 did not obviously modify their original V isotope signature. In combination with fresh MORB data, our results also indicate that the bulk ocean crust is homogeneous in δ^{51}V with an average of -0.85 ± 0.02‰ (2SE, $n = 53$).

5.3. Vanadium isotope fractionation during magmatic differentiation at MOR

The δ^{51}V values of the MOR lavas from the 9°N OSC on the EPR appear to increase with increasing degree of magma differentiation, as clearly shown by relationships of δ^{51}V with MgO and SiO_2 concentrations (Fig. 7 and Fig. 8). However, the volatile concentrations and δ^{18}O in 9°N OSC lavas also suggest that small extents of partial melting and crustal assimilation into a crystallizing magma chamber was a common process during their petrogenesis (Wanless et al., 2011). Thus we need to assess whether crustal assimilation is important for V isotopic variations observed on the MOR lavas. The first possible contaminant is oceanic sediments because large V isotope variations (up to 3‰) have been observed or predicted in supergene materials (Schuth et al., 2017; Ventura et al., 2015; Wu et al., 2015, 2016). However, variations in Sr, Nd, and Pb isotopic compositions of 9°N OSC andesites and dacites are limited and similar to the EPR and OSC N-MORB as shown by Wanless et al. (2010), suggesting that sediments were not involved in the formation of 9°N OSC high-silica andesites and dacites.

Previous petrogenetic models based on major and trace element compositions showed the partially melted AOC is the most likely source of the contaminant for the evolved lavas from 9°N OSC on the EPR (Wanless et al., 2010). As pointed out by Wilson et al. (2006), the concentrations for most major elements and fluid immobile trace elements of basaltic lavas from Site 1256 have values and ranges comparable to lavas from northern EPR, which indicates that similar processes operated at the superfast-spreading ridge to form Site 1256 and the modern EPR. The samples collected from Hole 1256D could thus be applied as the representative of the AOC component which was assimilated into the evolved lavas of 9°N OSC. As shown above, the AOC from site 1256 have restricted δ^{51}V variations similar to that of fresh EPR MORBs. Therefore, the AOC component could not produce the isotopic variations of the 9°N OSC evolved lavas.

From the above arguments, we propose that V isotope variations of the 9°N OSC lavas are best explained by crystal–liquid fractionation during magmatic differentiation, whereby the light V isotope (i.e., ^{50}V) is preferentially partitioned into crystallizing phases. For the 9°N OSC lavas, the steady decreases in CaO/Al_2O_3 in samples with MgO content below ~8 wt.% (Fig. 6), is a consequence of significant clinopyroxene fractionation-typical of many evolved MORB suites (e.g. Botcharnikov et al., 2008; Juster et al., 1989). There is also a significant inflection point in the trends of FeO^T and TiO_2 in these samples when MgO decreases below 5 wt.%, (Fig. 6). Their marked decrease can be attributed to initiation of crystallization of Fe–Ti oxides such as (titano)magnetite and ilmenite (e.g. Juster et al., 1989). The evolved OSC samples show a decrease in V content at ~8 wt% MgO (Fig. 5), suggesting that clinopyroxene is the primary fractionating mineral phase to host V during magmatic differentiation before the saturation and crystallization of Fe–Ti oxide (e.g. Lee et al., 2005). And Fe–Ti oxides are the main mineral phases to host V when they start to crystallize (e.g. Jenner et al., 2015). The evolved samples also show obvious shifts towards higher δ^{51}V between 4 wt.% < MgO < 6 wt.% (Fig. 6), suggesting that clinopyroxene and Fe–Ti oxides preferentially depleted ^{50}V from 9°N OSC lavas during crystallization.

Stable isotopes can be fractionated between species with different valence states and coordination numbers (CN) because of the variable bond strengths (e.g. Bigeleisen and Mayer, 1947). Recent calculations showed that V species with higher valence state and lower CN tend to be enriched in ^{51}V (Wu et al., 2015). In magmatic systems on Earth, V exists as a mixture of V^{3+}, V^{4+}, and V^{5+}. Experimental studies have shown that V is more incompatible with increasing valence in clinopyroxene and Fe–Ti oxides (e.g. Toplis and Corgne, 2002; Mallmann and O'Neill, 2009). Furthermore, both V^{3+} and V^{4+} prefer the octahedral coordination sites in pyroxene and Fe–Ti oxides with CN of six (Papike et al., 2005), while the CN of V^{5+} is lower than six in silicate melts because of the existence of 4-fold and 5-fold coordinated V^{5+} (Sutton et al., 2005). Thus ^{50}V should be enriched in clinopyroxene and Fe–Ti oxides, which prefer to incorporate V with lower valence state and higher CN during crystallization from silicate melts. This is consistent with our observations that δ^{51}V shifts towards higher values with decreasing MgO content (Fig. 7).

Calculations using Rhyolite MELTS software (Gualda and Ghiorso, 2014) were applied to simulate the crystallization process in 9°N OSC lavas. A relatively primitive basaltic sample from the 9°N OSC with MgO of ~8 wt.% (Wanless et al., 2012) was used as the starting melt composition. Pressure was set at 1 kbar, the fO_2 was set at the quartz–fayalite–magnetite (QFM) buffer which is typical for the MORBs (e.g. Cottrell and Kelley, 2011). The temperature in the calculation decreases from the liquidus

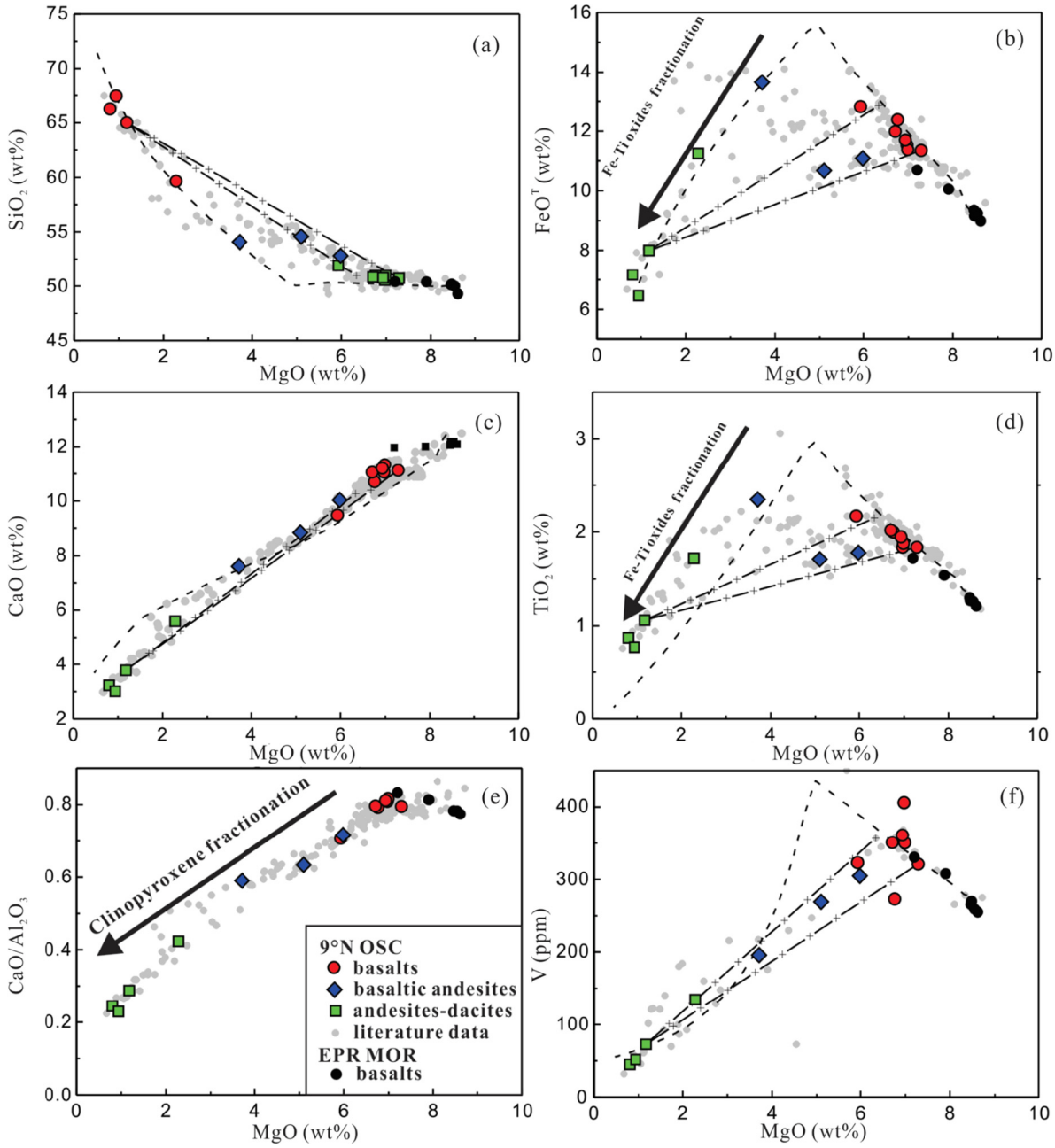

Fig. 6. MgO versus (a) SiO_2, (b) FeO^T, (c) CaO, (d) TiO_2, (e) CaO/Al_2O_3 and (d) V in the studied lava samples from the 9°N OSC and fresh MORB from the East Pacific Rise (EPR). The 9°N OSC data are from Wanless et al. (2010) and Wanless et al. (2012), and the studied EPR MORB data are from Sims et al. (2003) and Perfit et al. (2012). Modeled major element variations of silicic magmas during differentiation. Liquid lines of descent (dash line) are calculated using rhyolite-MELTS at $P = 1$ kbar and $fO_2 =$ FMQ. The temperature in the calculation decreases from the liquidus of 1200 °C to 900 °C in increments of 4 °C. The partition coefficients of V between melts and minerals were: ${}^{\text{pyroxene/melt}}D_V = 1.2$, ${}^{\text{Fe–Ti oxide/melt}}D_V = 17$, and ${}^{\text{Plagioclase/melt}}D_V = 0$. Solid black lines show binary mixing trends between a high-silica dacite and two different basaltic compositions, including a ferrobasalt and a FeTi basalt from the OSC. Crosses represent 10% mixing intervals. The inflection in the differentiation trend of CaO/Al_2O_3 at ~8 wt.% MgO is due to fractionation of clinopyroxene. The inflection of FeO^T and TiO_2 at ~5 wt.% MgO is attributed to fractionation of magnetite.

(1200 °C) to 900 °C at an increment of 4 °C. To model the variations of V, we set the partition coefficient of V (${}^{\text{cpx/melt}}D_V = 1.2$, ${}^{\text{oxide/melt}}D_V = 17$, ${}^{\text{plag/melt}}D_V = 0$) based on the experimental results conducted around the QFM buffer (Toplis and Corgne, 2002; Mallmann and O'Neill, 2009). Model results show that the major element and V compositions similar to those of 9°N OSC basalts and high silica lavas (andesites and dacites) can be obtained through 85~90% crystal fractionation of a MORB magma (Fig. 6). However, the calculated compositions, particularly FeO^T, TiO_2 and V, of moderately differentiated basaltic andesites deviate from expected by simple crystal fractionation (Fig. 6).

Magma mixing has been proposed to play an important role in the formation of basaltic andesites and low-FeO andesites from 9°N OSC (Wanless et al., 2012). Binary mixing between high-silica dacite and basalt can explain the compositions including V of the moderately evolved lavas (Fig. 6). Thus magma mixing might also play roles in controlling the V isotope composition of 9°N OSC lavas, especially the basaltic andesites, which we will consider below.

To quantitatively address the effect of crystal fractionation on $\delta^{51}V$, we use the same Rhyolite MELTS model to simulate V isotope fractionations in 9°N OSC lavas. V isotopic evolution trends for melts were subsequently calculated with variable $\Delta^{51}V_{\text{mineral-melt}}$

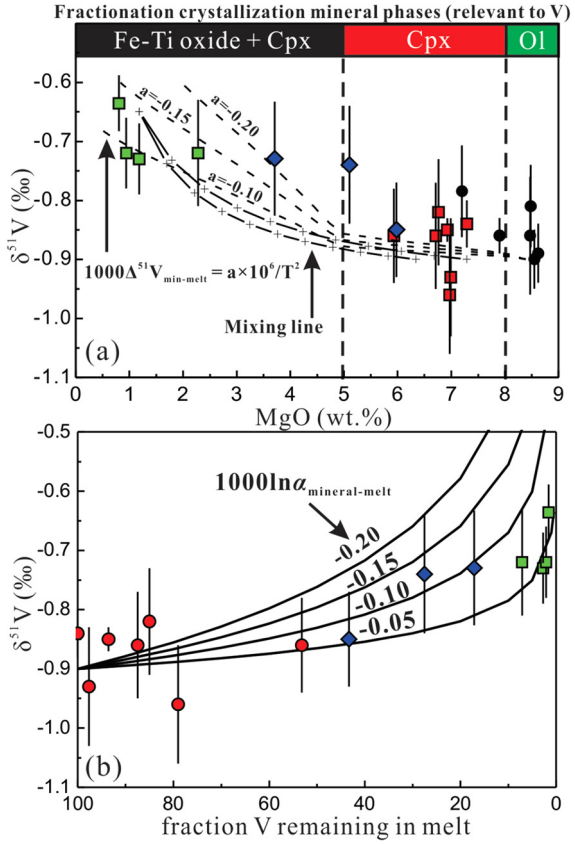

Fig. 7. (a) MgO versus δ^{51}V in the studied lava samples at 9°N OSC and fresh MORBs at EPR. Samples with MgO > ~8 wt.% reflect fractional crystallization of olivine, followed by clinopyroxene (MgO < ~8 wt.%), and Fe–Ti oxides (MgO < ~5 wt.%) as indicated by Fig. 6. Modeling of V isotopic fractionation of silicic magmas during differentiation. The crystallizing mineral modes at each stage along the liquidus line of descent are first modeled based on the results from rhyolite-MELTS with the same input parameters as provided in Fig. 6. The starting δ^{51}V is set as −0.90‰ based on the 9°N OSC basalts. Liquid V isotopic evolution trends with variable $\Delta^{51}V_{mineral\text{-}melt}$ are shown. The 9°N OSC and EPR data plotted here, are best fit with $\Delta^{51}V_{mineral\text{-}melt} = -0.15 \times 10^6/T^2$. Solid black lines show binary mixing trends also with input parameters the same as provided in Fig. 6, and setting the endmember V isotope of −0.9‰ (basalt) and −0.65‰ (dacite). (b) Rayleigh fractionation calculations of the V isotope evolution in 9°N OSC. Curves in (b) are for different bulk fractionation factors. The starting δ^{51}V is −0.90‰. Ba content is used as a proxy for melt fraction and basalt sample 266-33 as the starting melt composition. The model shows that a $\Delta^{51}V_{solid\text{-}melt}$ of about −0.1‰ is quite consistent with the 9°N OSC lava data.

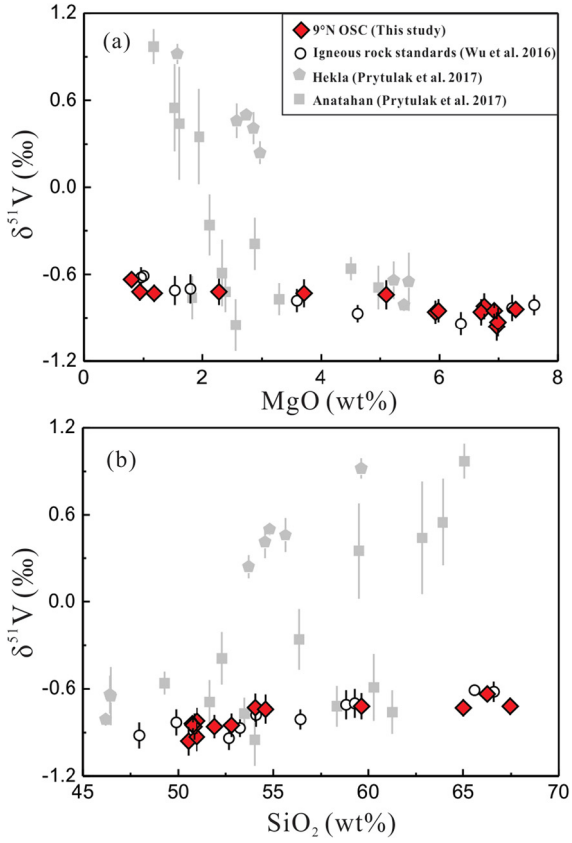

Fig. 8. Vanadium isotopic variations along with (a) MgO and (b) SiO_2 in Hekla and Anatahan volcanic rocks from Prytulak et al. (2017), igneous rock standards from Wu et al. (2016), and 9°N OSC lavas from this study.

(Fig. 7). Binary mixing lines are also calculated to evaluate the role of magma mixing (Fig. 7). Model results show that magma mixing could not explain the V isotope variations of 9°N OSC lavas. In contrast, the fractional crystallization model using $\Delta^{51}V_{mineral\text{-}melt} = -0.15 \times 10^6/T^2$ are more consistent with the V isotope variations in 9°N OSC lavas (Fig. 7).

The Rayleigh fractionation calculation was also applied to estimate the bulk V isotope fractionation factor during crystallization. The change in abundance of highly incompatible elements has previously been used to estimate the fraction of melt remaining in evolving magmatic systems (e.g. Savage et al., 2011; Prytulak et al., 2017). Here we use the Ba content as a proxy for the fraction of melt remaining. Vanadium isotopic compositions are plotted against the total proportion of V remaining in the melt with different bulk fractionation factors in Fig. 7. Our model shows that the V isotope variations of the 9°N OSC samples can be explained with $\Delta^{51}V_{solid\text{-}melt}$ at about −0.1‰ (Fig. 7), consistent with the results based on MELTS model above. Consequently, a bulk $\Delta^{51}V_{solid\text{-}melt}$ value of ~−0.1‰ can be inferred from the magmatic system at the 9°N OSC.

5.4. Controlling factors of V isotope fractionation during magmatism

5.4.1. The effect of oceanic crustal melting and assimilation

As discussed above, ^{51}V prefers the melt relative to mineral phases during magmatic differentiation. As Fig. 8 shows, the direction of isotope fractionation is consistent with previous studies on igneous rock standards and lavas from Anatahan and Hekla (Wu et al., 2016; Prytulak et al., 2017; Williams et al., 2018), which implies that such evolution trend may be applicable to other magmatic systems and not just limited to the case of 9°N OSC lavas. However, the magnitude of V isotope variations in 9°N OSC lavas is much smaller than the Anatahan and Hekla cases although they have similar ranges of MgO and SiO_2 contents (Fig. 8). Notably, the bulk $\Delta^{51}V_{solid\text{-}melt}$ value of about −0.1‰ can explain the observation at 9°N OSC lavas, while studies on Anatahan and Hekla suites suggest bulk $\Delta^{51}V_{solid\text{-}melt}$ of about −0.4 to −0.5‰ (Prytulak et al., 2017). Clearly, $\Delta^{51}V_{solid\text{-}melt}$ dramatically varies in different magma systems with distinct controlling factors. Since assimilation along with fractional crystallization is thought to occur during the formation of dacite of 9°N OSC, we will first evaluate if the smaller isotopic fractionation in 9°N OSC than the case of Anatahan and Hekla suites could be explained by assimilation.

Detailed petrological models have shown that the high silica dacite can be formed by extensive fractional crystallization (73~85% fractional crystallization) with the assimilation of AOC melted to small extents (1~15%) (Wanless et al., 2010). Both observation and experimental studies showed that the product from low proportion melting of AOC is high silica melt with low V content (<100 ppm, e.g. France et al., 2014). In addition, partial melting experiments were conducted to simulate anatectic processes occurring at the roof of fast-spreading oceanic ridge magma chambers (Erdmann et al., 2015, 2017), i.e. the specific process

that is thought to occur at 9°N OSC. Here, we model the V isotope composition of the partially melted AOC products based on the results of partial melting experimental studies (Erdmann et al., 2015, 2017) with various $\Delta^{51}V_{solid\text{-}melt}$ assuming that isotope equilibrium is achieved during partial melting. The modeling results in Fig. S1 show that if we assume a V isotope fractionation factor ($\Delta^{51}V_{mineral\text{-}melt} = -0.75 \times 10^6/T^2$) as presented by Prytulak et al. (2017) to control the fractionation of MOR samples, the end-members forming the evolved MOR samples should both have $\delta^{51}V$ much higher than what we observed (Fig. S1). In addition, it is generally thought that either magma mixing (Sigmarsson et al., 1992) or assimilation and fractional crystallization (Chekol et al., 2011) is important to form the Hekla high-silica lava. Thus it is difficult to ascribe the smaller degree of isotopic fractionation in 9°N OSC relative to Hekla as the results of assimilation/mixing. Otherwise, our models explicitly prove that the observed trend resulted from V isotope fractionation during melt-solid segregation, which has fractionation factor ($\Delta^{51}V_{mineral\text{-}melt} = -0.15 \times 10^6/T^2$) much smaller than that determined by Prytulak et al. (2017) (Fig. S1).

5.4.2. The effect of crystallizing mineral phase on $\delta^{51}V$ of MORB

The proportions and order of crystallization of minerals in each of the rock suites discussed above might potentially explain their geochemical variations, however, this is not the case for the observed V isotope systematics. This is because the main mineral phases that control V isotope variations of 9°N OSC suite are pyroxenes and Fe–Ti oxides, which are identical to those in the Hekla and Anatahan suites (Prytulak et al., 2017). In addition, the bonding environments of both V^{3+} and V^{4+} are analogous in pyroxenes and Fe–Ti oxides (magnetite and ilmenite), as they likely occupy octahedral sites in these minerals (Papike et al., 2005). Thus, the force constant of V–O bonds with same valence state of V should be similar to these of pyroxenes and Fe–Ti oxides (e.g. Sossi and O'Neill, 2017). More importantly, Fe–Ti oxides are the most important mineral controlling the V content and isotope composition of V in melts because V is highly compatible in Fe–Ti oxides. Thus, in both our study and Prytulak et al. (2017), the fractionation models were run with same $\Delta^{51}V_{mineral\text{-}melt}$ value for both Fe–Ti oxide and pyroxene as a first order assumption. And the change of the $\Delta^{51}V_{mineral\text{-}melt}$ value of pyroxene will not obviously modify the differentiation trend of V for the igneous rock series in our study and Prytulak et al. (2017). Therefore, we conclude that the modal proportion is not the main factor that leads to the different $\Delta^{51}V_{solid\text{-}melt}$ among 9°N OSC, Hekla and Anatahan suites.

5.4.3. The effect of fO_2 on V isotope fractionation

It is well known that fO_2 controls valence states, CN, and partitioning of V in both melts and minerals (e.g. Toplis and Corgne, 2002; Papike et al., 2005; Mallmann and O'Neill, 2009). Since the fO_2 of Anatahan basalts is about 2 log units more oxidized (FMQ ~+2, De Moor et al., 2005) compared to MORB at 9°N OSC (FMQ ~0, Wanless et al., 2010), the different isotope trends between the 9°N OSC and Anatahan suites might reflect the different redox conditions during crystallization given their different tectonomagmatic origins. Here we quantitatively explore the effect of fO_2 on equilibrium fractionation of V isotopes during magmatism.

First, we calculate the proportions of V with different valence states in melts under various fO_2. The existence of V^{2+} in melts was not considered because V^{2+} is negligible in the magmatic systems at the fO_2 range of the Earth. The relative proportions of V^{3+}, V^{4+}, and V^{5+} in melts at fO_2 from FMQ-3 to FMQ+3 were calculated based on the thermodynamic model by Toplis and Corgne (2002). Because V isotope variations mainly occur among andesitic to dacitic rocks, the starting composition of basaltic andesite 265-24 at 9°N OSC was applied for the calculation. The temperature is set at 1000 °C. The results in Fig. 9 show that V^{3+} is the minor valence state with fO_2 from FMQ-3 to FMQ+3, while V^{4+} is the dominant valence state when fO_2 is below FMQ+2. The proportion of V^{5+} increases with increasing of fO_2, until V^{5+} becomes the dominant valence state of vanadium at fO_2 above FMQ+2.

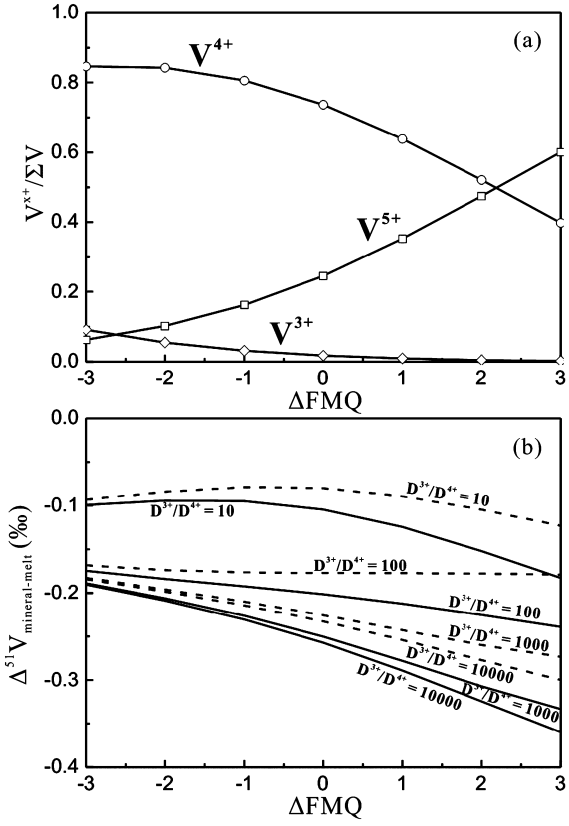

Fig. 9. (a) Calculated variations of the relative proportions of V^{n+} as a function of fO_2 for the composition of basaltic andesite 265-24 at 1000 °C. (b) Modeling for variations of V isotope fractionation factors between mineral and silicate melts ($\Delta^{51}V_{mineral\text{-}melt}$) with fO_2 change. Dashed curves denote the model results assuming $\Delta^{51}V_{V^{3+}\text{-}V^{4+}} = -0.19‰$ and $\Delta^{51}V_{V^{3+}\text{-}V^{5+}} = -0.38‰$. Solid curves denote the model results assuming $\Delta^{51}V_{V^{3+}\text{-}V^{4+}} = -0.19‰$ and $\Delta^{51}V_{V^{3+}\text{-}V^{5+}} = -0.48‰$. Curve labels denote the input ratios of D^{3+}/D^{4+} (see text for further details).

The proportions of V^{3+}, V^{4+} and V^{5+} in minerals are calculated by assuming the minerals are in equilibrium with ambient melts. The partition coefficient for an individual valence state is defined as: $D^{VX+} = V^{X+}{}_{mineral}/V^{X+}{}_{melt}$. Because V^{5+} is highly incompatible in the main rock-forming minerals (including clinopyroxene and Fe–Ti oxide) (e.g. Toplis and Corgne, 2002; Papike et al., 2005), we assume that V^{5+} is not incorporated into these minerals ($D^{V^{5+}} = 0$). Therefore, the proportion of V^{3+} and V^{4+} in minerals depends on the ratio of partition coefficient of V^{3+} and V^{4+} ($D^{V^{3+}}/D^{V^{4+}}$). The proportions of V^{3+} and V^{4+} in minerals are therefore:

$$\left(V^{3+}/V^{4+}\right)_{mineral} = \left(V^{3+}/V^{4+}\right)_{melt} \times \left(D^{V^{3+}}/D^{V^{4+}}\right). \quad (2)$$

Because the plausible ratios of D^{V3+}/D^{V4+} between Fe–Ti oxide/clinopyroxene and melt generally vary from 100 to 1000 (Toplis and Corgne, 2002), we assume a larger range of $D^{V^{3+}}/D^{V^{4+}}$ from 10 to 10000 in order to fully cover the natural variation. Consequently, the variation of $\Delta^{51}V_{mineral\text{-}melt}$ with the change of redox conditions can be calculated if we know the equilibrium isotopic fractionation among V^{3+}, V^{4+}, and V^{5+} in minerals and melts.

The equilibrium isotopic fractionation factors among V^{3+}, V^{4+}, and V^{5+} in minerals and liquid silicates at magmatic temperatures have not yet been reported. Although the structure of silicate melt

is distinct from that of aqueous solution, given that the coordination environments of V (i.e. V–O bonding) in solutions are similar to that in silicate melts, isotope fractionation among V species in aqueous solutions can be used as a good approximation to the case in silicate melts. Thus we can extrapolate the theoretical results for V isotope fractionation among V^{3+}, V^{4+}, and V^{5+} in solution systems from Wu et al. (2015) to magmatic systems at high temperature. In silicate melts, V^{3+} and V^{4+} exist in octahedral geometry with V–O CN of six (Sutton et al., 2005). Hence, we set the isotope fractionation factor between six-fold V^{3+} and six-fold V^{4+} in liquid silicates based on the results of Wu et al. (2015) at 1000 °C, i.e. −0.19‰. Because spectral studies imply that the CN of V^{5+} is between four and six in liquid silicates (Righter et al., 2006; Sutton et al., 2005), the results of six-fold V^{5+} and four-fold V^{5+} are both applied to model the redox-controlling V isotope fractionation between mineral and melt. Similarly, using the results of Wu et al. (2015) at 1000°C, we determine that $\Delta^{51}V$ between six-fold V^{3+} and six-fold V^{5+} is −0.38‰, and $\Delta^{51}V$ between six-fold V^{3+} and four-fold V^{5+} is −0.48‰.

Recent experimental studies show that Fe isotope fractionation is negligible between Fe^{2+} in fluids and minerals with same CN of Fe, implying that fluids and minerals have similar bonding energy for Fe^{2+}-O (Sossi and O'Neill, 2017). Assuming that such a rule is also valid in the V isotope system, we could predict that the reduced partition function ratios (β-factors) of V^{3+} and V^{4+} in silicate liquids and minerals are identical because they all occupy octahedral sites in both melts and main rock-forming minerals (Papike et al., 2005; Sutton et al., 2005). In addition, because V^{5+} is highly incompatible in silicate minerals, we do not consider the effect of V^{5+} in minerals on isotope fractionation.

Variations of $\Delta^{51}V_{\text{mineral-melt}}$ with fO_2 can be calculated on the basis of the assumptions above. The calculation details are presented in the Supplementary materials. As shown in Fig. 9, our models predict that $\Delta^{51}V_{\text{mineral-melt}}$ is about −0.2‰ at fO_2 of FMQ with the $D^{V^{3+}}/D^{V^{4+}}$ between 100 and 1000. Although this value is slightly larger than the $\Delta^{51}V_{\text{mineral-melt}}$ value (about −0.1‰) that is needed to explain the 9°N OSC evolution suite, this model shows that the absolute value of $\Delta^{51}V_{\text{mineral-melt}}$ increases with increasing ambient fO_2, which is consistent with the larger magnitude of V isotope variations in the Anatahan suite than in the 9°N OSC lavas. However, under the fO_2 for oceanic basalts (from FMQ-0.5 to FMQ+2.5, Cottrell and Kelley, 2011; Kelley and Cottrell, 2009), the estimated range of $\Delta^{51}V_{\text{mineral-melt}}$ is around 0.1‰, much smaller than the observed difference of $\Delta^{51}V_{\text{mineral-melt}}$ between the 9°N OSC and Anatahan lava systems, i.e. 0.3 to 0.4‰. Such discrepancy cannot be reconciled with the equilibrium isotopic fractionation factors among V^{3+}, V^{4+} and V^{5+} in minerals and liquid silicates estimated in our model. In addition, the larger fractionation factor for Hekla than 9°N OSC suite cannot be explained by redox control because they have similar fO_2 (Moune et al., 2007; Wanless et al., 2010).

Consequently, our model implies that redox conditions play important roles in controlling V isotope fractionation during magma differentiation because the partitioning and proportion of multivalent V species with different isotopic compositions is a function of fO_2. This conclusion is consistent with recent experimental studies (Sossi et al., 2018), although our observed $\Delta^{51}V_{\text{mineral-melt}}$ is smaller than $\Delta^{51}V_{\text{magnetite-melt}}$ of the experimental results, which might be caused by the melt composition difference between natural and experimental system. The large $\Delta^{51}V_{\text{mineral-melt}}$ variations based on our results cannot be entirely ascribed to these factors. More observations are necessary to ascertain the V isotopic variations during magmatic evolution. Further experimental studies are also needed to better understand the magnitude and mechanism of mineral-melt and inter-mineral V isotope fractionation. Despite these uncertainties, our work clearly shows that V isotopic fractionation is sensitive to the redox conditions during magmatism, and V isotopes can serve as a tracer of fO_2 variation during magmatic processes.

6. Conclusions

(1) Our analyses of fresh MORB provide the best constraints on the V isotope composition of MORBs, i.e. -0.84 ± 0.02‰ (2SE, $n = 22$). The mean $\delta^{51}V$ of individual ridge segments is correlate with ridge depth and melt composition, reflecting the effect of extents of melting on V isotope fractionation during mantle melting. This may resolve the apparent discrepancies between the present results and the earlier work of Prytulak et al. (2013).

(2) Altered basalts and gabbros from the intact oceanic crust at IODP Site 1256 have a small variation of $\delta^{51}V$ with an average of -0.85 ± 0.11‰ (2SD, $n = 31$), identical to that of fresh MORB. This observation suggests that the AOC has homogeneous $\delta^{51}V$ regardless of alteration at different temperatures and water–rock ratios.

(3) Evolved MOR lavas from the 9°N OSC on the EPR show apparent shifts towards heavier $\delta^{51}V$ with increasing differentiation. Removal of clinopyroxene and Fe–Ti oxide during crystallization likely results in heavier isotopic compositions in evolved magmas compared to typical MORB. The V isotope variations can be described by a $\Delta^{51}V_{\text{mineral-melt}} = -0.15 \times 10^6/T^2$.

(4) The magnitude of V isotope variations in 9°N OSC lavas is much smaller than that of lavas from Anatahan Island (Marianas) and Hekla Volcano (Iceland) reported by Prytulak et al. (2017) although they have similar ranges of MgO and SiO_2 contents. Our fractionation models show that redox condition is important for controlling V isotope fractionation. However the $\Delta^{51}V_{\text{mineral-melt}}$ difference among these results cannot be solely ascribed to redox variation. Further studies are helpful to understand the controlling factors for V isotope fractionation in magmatic system. Nonetheless, our study shows the great potential to apply V stable isotopes as a redox tracer for magmatism.

Acknowledgements

This study was supported by National Science Foundation of China (41630206 and 41325011), the Strategic Priority Research Program (B) of the Chinese Academy of Sciences (XDB18010101), and the 111 Project. We thank Shengyu Tian and Zhenhui Hou for help with the analyses. NSF supported the analytical studies of the 9°N OSC lavas through grant OCE-0527075 to Perfit and Wanless. We are grateful to the editorial handling of Dr. Frederic Moynier and constructive comments from two anonymous reviewers.

Appendix A. Supplementary material

Supplementary material related to this article can be found online at https://doi.org/10.1016/j.epsl.2018.04.009.

References

Alt, J.C., Laverne, C., Coggon, R.M., Teagle, D.A., Banerjee, N.R., Morgan, S., Smith-Duque, C.E., Harris, M., Galli, L., 2010. Subsurface structure of a submarine hydrothermal system in ocean crust formed at the East Pacific Rise, ODP/IODP Site 1256. Geochem. Geophys. Geosyst. 11.

Alt, J.C., Teagle, D.A., 2000. Hydrothermal alteration and fluid fluxes in ophiolites and oceanic crust. Spec. Pap., Geol. Soc. Am. 349, 273–282.

Bigeleisen, J., Mayer, M.G., 1947. Calculation of equilibrium constants for isotopic exchange reactions. J. Chem. Phys. 15, 261–267.

Botcharnikov, R., Almeev, R., Koepke, J., Holtz, F., 2008. Phase relations and liquid lines of descent in hydrous ferrobasalt – implications for the Skaergaard intrusion and Columbia River flood basalts. J. Petrol. 49, 1687–1727.

Carbotte, S., Macdonald, K., 1992. East Pacific Rise 8–10 30′N: evolution of ridge segments and discontinuities from SeaMARC II and three-dimensional magnetic studies. J. Geophys. Res., Solid Earth 97, 6959–6982.

Chekol, T.A., Kobayashi, K., Yokoyama, T., Sakaguchi, C., Nakamura, E., 2011. Timescales of magma differentiation from basalt to andesite beneath Hekla Volcano, Iceland: constraints from U-series disequilibria in lavas from the last quarter-millennium flows. Geochim. Cosmochim. Acta 75, 256–283.
Cottrell, E., Kelley, K.A., 2011. The oxidation state of Fe in MORB glasses and the oxygen fugacity of the upper mantle. Earth Planet. Sci. Lett. 305, 270–282.
Dalton, C.A., Langmuir, C.H., Gale, A., 2014. Geophysical and geochemical evidence for deep temperature variations beneath mid-ocean ridges. Science 344, 80–83.
De Moor, J., Fischer, T., Hilton, D., Hauri, E., Jaffe, L., Camacho, J., 2005. Degassing at Anatahan volcano during the May 2003 eruption: implications from petrology, ash leachates, and SO_2 emissions. J. Volcanol. Geotherm. Res. 146, 117–138.
Eiler, J.M., Schiano, P., Kitchen, N., Stolper, E.M., 2000. Oxygen-isotope evidence for recycled crust in the sources of mid-ocean-ridge basalts. Nature 403, 530.
Erdmann, M., Fischer, L.A., France, L., Zhang, C., Godard, M., Koepke, J., 2015. Anatexis at the roof of an oceanic magma chamber at IODP Site 1256 (equatorial Pacific): an experimental study. Contrib. Mineral. Petrol. 169, 39.
Erdmann, M., France, L., Fischer, L.A., Deloule, E., Koepke, J., 2017. Trace elements in anatectic products at the roof of mid-ocean ridge magma chambers: an experimental study. Chem. Geol. 456, 43–57.
Fisk, M., Kelley, K.A., 2002. Probing the Pacific's oldest MORB glass: mantle chemistry and melting conditions during the birth of the Pacific Plate. Earth Planet. Sci. Lett. 202, 741–752.
France, L., Koepke, J., MacLeod, C.J., Ildefonse, B., Godard, M., Deloule, E., 2014. Contamination of MORB by anatexis of magma chamber roof rocks: constraints from a geochemical study of experimental melts and associated residues. Lithos 202, 120–137.
Gale, A., Dalton, C.A., Langmuir, C.H., Su, Y., Schilling, J.G., 2013. The mean composition of ocean ridge basalts. Geochem. Geophys. Geosyst. 14, 489–518.
Gale, A., Langmuir, C.H., Dalton, C.A., 2014. The global systematics of ocean ridge basalts and their origin. J. Petrol. 55, 1051–1082.
Gannoun, A., Burton, K.W., Parkinson, I.J., Alard, O., Schiano, P., Thomas, L.E., 2007. The scale and origin of the osmium isotope variations in mid-ocean ridge basalts. Earth Planet. Sci. Lett. 259, 541–556.
Gao, Y., Casey, J.F., Bernardo, L.M., Yang, W., Bissada, K.A., 2018. Vanadium isotope composition of crude oil: effects of source, maturation and biodegradation. Geol. Soc. (Lond.) Spec. Publ. 468 (1), 83–103.
Gao, Y., Huang, J., Casey, J.F., 2009. Data report: trace element geochemistry of oceanic crust formed at superfast-spreading ridge, Hole 1256D. In: Proc. IODP 309, p. 312.
Gao, Y., Vils, F., Cooper, K., Banerjee, N., Harris, M., Hoefs, J., Teagle, D., Casey, J., Elliott, T., Laverne, C., 2012. Downhole variation of lithium and oxygen isotopic compositions of oceanic crust at East Pacific Rise, ODP Site 1256. Geochem. Geophys. Geosyst. 13.
Gualda, G.A., Ghiorso, M.S., 2014. Phase-equilibrium geobarometers for silicic rocks based on rhyolite-MELTS, part 1: principles, procedures, and evaluation of the method. Contrib. Mineral. Petrol. 168, 1033.
Huang, J.-H., Huang, F., Evans, L., Glasauer, S., 2015. Vanadium: global (bio)geochemistry. Chem. Geol. 417, 68–89.
Jenner, F.E., Hauri, E.H., Bullock, E.S., König, S., Arculus, R.J., Mavrogenes, J.A., Mikkelson, N., Goddard, C., 2015. The competing effects of sulfide saturation versus degassing on the behavior of the chalcophile elements during the differentiation of hydrous melts. Geochem. Geophys. Geosyst. 16, 1490–1507.
Juster, T.C., Grove, T.L., Perfit, M.R., 1989. Experimental constraints on the generation of FeTi basalts, andesites, and rhyodacites at the Galapagos Spreading Center, 85 W and 95 W. J. Geophys. Res., Solid Earth 94, 9251–9274.
Karner, J., Papike, J.J., Shearer, C.K., 2006. Comparative planetary mineralogy: pyroxene major- and minor-element chemistry and partitioning of vanadium between pyroxene and melt in planetary basalts. Am. Mineral. 91, 1574–1582.
Kelley, K.A., Cottrell, E., 2009. Water and the oxidation state of subduction zone magmas. Science 325, 605–607.
Kent, G., Singh, S., Harding, A., Sinha, M., Orcutt, J., Barton, P., White, R., Bazin, S., Hobbs, R., Tong, C., 2000. Evidence from three-dimensional seismic reflectivity images for enhanced melt supply beneath mid-ocean-ridge discontinuities. Nature 406, 614–618.
Klein, E.M., Langmuir, C.H., 1987. Global correlations of ocean ridge basalt chemistry with axial depth and crustal thickness. J. Geophys. Res., Solid Earth 92, 8089–8115.
Koepke, J., Christie, D., Dziony, W., Holtz, F., Lattard, D., Maclennan, J., Park, S., Scheibner, B., Yamasaki, T., Yamazaki, S., 2008. Petrography of the dike–gabbro transition at IODP Site 1256 (equatorial Pacific): the evolution of the granoblastic dikes. Geochem. Geophys. Geosyst. 9.
Laubier, M., Grove, T.L., Langmuir, C.H., 2014. Trace element mineral/melt partitioning for basaltic and basaltic andesitic melts: an experimental and laser ICP-MS study with application to the oxidation state of mantle source regions. Earth Planet. Sci. Lett. 392, 265–278.
Lee, C.-t.A., Leeman, W.P., Canil, D., Li, Z.-X.A., 2005. Similar V/Sc systematics in MORB and arc basalts: implications for the oxygen fugacities of their mantle source regions. J. Petrol. 46, 2313–2336.
Mallmann, G., O'Neill, H.S.C., 2009. The crystal/melt partitioning of V during mantle melting as a function of oxygen fugacity compared with some other elements (Al, P, Ca, Sc, Ti, Cr, Fe, Ga, Y, Zr and Nb). J. Petrol. 50, 1765–1794.
Moune, S., Sigmarsson, O., Thordarson, T., Gauthier, P.-J., 2007. Recent volatile evolution in the magmatic system of Hekla volcano, Iceland. Earth Planet. Sci. Lett. 255, 373–389.
Neo, N., Yamazaki, S., Miyashita, S., 2009. Data report: bulk rock compositions of samples from the IODP Expedition 309/312 sample pool, ODP Hole 1256D. In: Teagle, D.A.H., Alt, J.C., Umino, S., Miyashita, S., Banerjee, N.R., Wilson, D.S. (Eds.), The Expedition 309/312.
Nielsen, S.G., Owens, J.D., Horner, T.J., 2016. Analysis of high-precision vanadium isotope ratios by medium resolution MC-ICP-MS. J. Anal. At. Spectrom. 31 (2), 531–536. https://doi.org/10.1039/C5JA00397K.
Nielsen, S.G., Prytulak, J., Halliday, A.N., 2011. Determination of precise and accurate $^{51}V/^{50}V$ isotope ratios by MC-ICP-MS, part 1: chemical separation of vanadium and mass spectrometric protocols. Geostand. Geoanal. Res. 35, 293–306.
Papike, J.J., Karner, J.M., Shearer, C.K., 2005. Comparative planetary mineralogy: valence state partitioning of Cr, Fe, Ti, and V among crystallographic sites in olivine, pyroxene, and spinel from planetary basalts. Am. Mineral. 90, 277–290.
Perfit, M.R., Wanless, V.D., Ridley, W.I., Klein, E.M., Smith, M.C., Goss, A.R., Hinds, J.S., Kutza, S.W., Fornari, D.J., 2012. Lava geochemistry as a probe into crustal formation at the East Pacific Rise. Oceanography 25, 89–93.
Prytulak, J., Nielsen, S.G., Halliday, A.N., 2011. Determination of precise and accurate $^{51}V/^{50}V$ isotope ratios by multi-collector ICP-MS, part 2: isotopic composition of six reference materials plus the Allende chondrite and verification tests. Geostand. Geoanal. Res. 35, 307–318.
Prytulak, J., Nielsen, S.G., Ionov, D.A., Halliday, A.N., Harvey, J., Kelley, K.A., Niu, Y.L., Peate, D.W., Shimizu, K., Sims, K.W.W., 2013. The stable vanadium isotope composition of the mantle and mafic lavas. Earth Planet. Sci. Lett. 365, 177–189.
Prytulak, J., Sossi, P.A., Halliday, A.N., Plank, T., Savage, P.S., Woodhead, J.D., 2017. Stable vanadium isotopes as a redox proxy in magmatic systems? Geochem. Perspect. Lett. 3, 75–84.
Righter, K., Sutton, S.R., Danielson, L., Pando, K., Newville, M., 2016. Redox variations in the inner solar system with new constraints from vanadium XANES in spinels. Am. Mineral. 101, 1928–1942.
Righter, K., Sutton, S.R., Newville, M., Le, L., Schwandt, C.S., Uchida, H., Lavina, B., Downs, R.T., 2006. An experimental study of the oxidation state of vanadium in spinel and basaltic melt with implications for the origin of planetary basalt. Am. Mineral. 91, 1643–1656.
Savage, P.S., Georg, R.B., Williams, H.M., Burton, K.W., Halliday, A.N., 2011. Silicon isotope fractionation during magmatic differentiation. Geochim. Cosmochim. Acta 75, 6124–6139.
Schauble, E., Rossman, G.R., Taylor Jr, H.P., 2004. Theoretical estimates of equilibrium chromium-isotope fractionations. Chem. Geol. 205, 99–114.
Schuth, S., Horn, I., Brüske, A., Wolff, P.E., Weyer, S., 2017. First vanadium isotope analyses of V-rich minerals by femtosecond laser ablation and solution-nebulization MC-ICP-MS. Ore Geol. Rev. 81, 1271–1286.
Sempere, J.C., Macdonald, K.C., 1986. Deep-tow studies of the overlapping spreading centers at 9 03′N on the East Pacific Rise. Tectonics 5, 881–900.
Seyfried, W.E., Mottl, M.J., 1982. Hydrothermal alteration of basalt by seawater under seawater-dominated conditions. Geochim. Cosmochim. Acta 46, 985–1002.
Siebert, J., Badro, J., Antonangeli, D., Ryerson, F.J., 2013. Terrestrial accretion under oxidizing conditions. Science, 1227923. https://doi.org/10.1126/science.1227923.
Sigmarsson, O., Condomines, M., Fourcade, S., 1992. A detailed Th, Sr and O isotope study of Hekla: differentiation processes in an Icelandic Volcano. Contrib. Mineral. Petrol. 112, 20–34.
Sims, K., Blichert-Toft, J., Fornari, D., Perfit, M., Goldstein, S., Johnson, P., DePaolo, D., Hart, S., Murrell, M., Michael, P., 2003. Aberrant youth: chemical and isotopic constraints on the origin of off-axis lavas from the East Pacific Rise, 9–10 N. Geochem. Geophys. Geosyst. 4.
Sossi, P.A., O'Neill, H.S.C., 2017. The effect of bonding environment on iron isotope fractionation between minerals at high temperature. Geochim. Cosmochim. Acta 196, 121–143.
Sossi, P.A., Prytulak, J., O'Neill, H.S.C., 2018. Experimental calibration of vanadium partitioning and stable isotope fractionation between hydrous granitic melt and magnetite at 800 °C and 0.5 GPa. Contrib. Mineral. Petrol. 173, 27.
Sutton, S.R., Karner, J., Papike, J., Delaney, J.S., Shearer, C., Newville, M., Eng, P., Rivers, M., Dyar, M.D., 2005. Vanadium K edge XANES of synthetic and natural basaltic glasses and application to microscale oxygen barometry. Geochim. Cosmochim. Acta 69, 2333–2348.
Teagle, D., Alt, J., Umino, S., Miyashita, S., Banerjee, N., Wilson, D., the Expedition 309/312 Scientists, 2006. Superfast spreading rate crust 2 and 3. Proc. Integr. Ocean Drill. Program 309/312, 50.
Toplis, M.J., Corgne, A., 2002. An experimental study of element partitioning between magnetite, clinopyroxene and iron-bearing silicate liquids with particular emphasis on vanadium. Contrib. Mineral. Petrol. 144, 22–37.
Ventura, G.T., Gall, L., Siebert, C., Prytulak, J., Szatmari, P., Hürlimann, M., Halliday, A.N., 2015. The stable isotope composition of vanadium, nickel, and molybdenum in crude oils. Appl. Geochem. 59, 104–117.
Wanless, V., Perfit, M., Klein, E., White, S., Ridley, W., 2012. Reconciling geochemical and geophysical observations of magma supply and melt distribution at the 9 N overlapping spreading center, East Pacific Rise. Geochem. Geophys. Geosyst. 13.

Wanless, V.D., Perfit, M.R., Ridley, W.I., Klein, E., 2010. Dacite petrogenesis on mid-ocean ridges: evidence for oceanic crustal melting and assimilation. J. Petrol. 51, 2377–2410.

Wanless, V.D., Perfit, M.R., Ridley, W.I., Wallace, P.J., Grimes, C.B., Klein, E.M., 2011. Volatile abundances and oxygen isotopes in basaltic to dacitic lavas on mid-ocean ridges: the role of assimilation at spreading centers. Chem. Geol. 287, 54–65.

White, W., Klein, E., 2014. 4.13 – Composition of the oceanic crust. In: Treatise on Geochemistry, second edition.

Williams, H.M., Prytulak, J., Woodhead, J.D., Kelley, K.A., Brounce, M., Plank, T., 2018. Interplay of crystal fractionation, sulfide saturation and oxygen fugacity on the iron isotope composition of arc lavas: an example from the Marianas. Geochim. Cosmochim. Acta 226, 224–243. https://doi.org/10.1016/j.gca.2018.02.008.

Wilson, D.S., Teagle, D.A., Alt, J.C., Banerjee, N.R., Umino, S., Miyashita, S., Acton, G.D., Anma, R., Barr, S.R., Belghoul, A., 2006. Drilling to gabbro in intact ocean crust. Science 312, 1016–1020.

Wu, F., Qi, Y., Yu, H., Tian, S., Hou, Z., Huang, F., 2016. Vanadium isotope measurement by MC-ICP-MS. Chem. Geol. 421, 17–25.

Wu, F., Qin, T., Li, X., Liu, Y., Huang, J.-H., Wu, Z., Huang, F., 2015. First-principles investigation of vanadium isotope fractionation in solution and during adsorption. Earth Planet. Sci. Lett. 426, 216–224.

Yamazaki, S., Neo, N., Miyashita, S., 2009. Data report: whole-rock major and trace elements and mineral compositions of the sheeted dike–gabbro transition in ODP Hole 1256D. In: Proc. IODP 309, p. 312.